ANALOG DEVICES
AHEAD OF WHAT'S POSSIBLE™

TECHNICAL ARTICLE

DESIGNING FOR LOW NOISE FEEDBACK CONTROL WITH MEMS GYROSCOPES

Mark Looney
Applications Engineer, Analog Devices, Inc.

Abstract

MEMS gyroscopes offer a simple way to measure angular rate of rotation, in packages that easily attach to printed circuit boards; so they are a popular choice to serve as the feedback sensing element in many different types of motion control systems. In this type of function, noise in the angular rate signals (MEMS gyroscope output) can have a direct influence over critical system behaviors, such as platform stability, and is often the defining factor in the level of precision that a control system can support. Therefore, low noise is a natural, guiding value for system architects and developers as they define and develop new motion control systems. Taking that value (low noise) a step further, translating critical system-level criteria, such as pointing accuracy, into noise metrics that are commonly available in MEMS gyroscope data sheets, is a very important part of early conceptual and architectural work. Understanding the system's dependence on gyroscope noise behaviors has a number of rewards, such as being able to establish relevant requirements for the feedback sensing element or, conversely, analyzing the system-level response to noise in a particular gyroscope. Once system designers have a good understanding of this relationship, they can focus on mastering the two key areas of influence that they have over the noise behaviors in their angular rate feedback loops: 1. developing the most appropriate criteria for MEMS gyroscope selection and 2. preserving the available noise performance throughout the sensor's integration process.

Motion Control Basics

Developing a useful relationship between the noise behaviors in a MEMS gyroscope and how it impacts key system behaviors often starts with a basic understanding of how the system works. Figure 1 offers an example architecture for a motion control system, which breaks the key system elements down into functional blocks. The functional objective for this type of system is to create a stable platform for personnel or equipment that can be sensitive to inertial motion. One example application is for a microwave antenna on an autonomous vehicle platform, which is maneuvering through rough conditions at a speed that causes abrupt changes in vehicle orientation. Without some real-time control of the pointing angle, these highly directional antennas may not be able to support continuous communication, while experiencing this type of inertial motion.

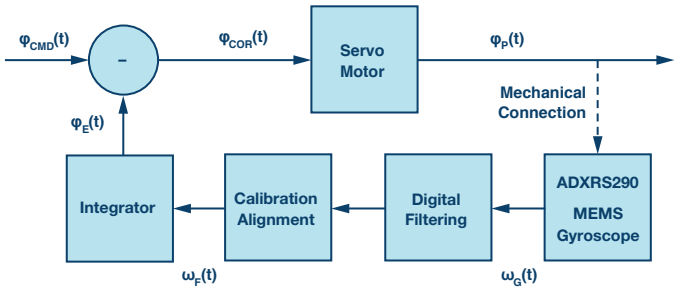

Figure 1. Example of a motion control system architecture.

The system in Figure 1 uses a servo motor, which will ideally rotate in a manner that is equal and opposite of the rotation that the rest of the system will experience. The feedback loop starts with a MEMS gyroscope, which observes the rate of rotation (φ_G) on the *stabilized platform*. The gyroscope's angular rate signals then feed into application-specific digital signal processing that includes filtering, calibration, alignment, and integration to produce real-time, orientation feedback, (φ_E). The servo motor's control signal (φ_{COR}) comes from a comparison of this feedback signal, with the *commanded* orientation (φ_{CMD}), which may come from a central mission control system or simply represent the orientation that supports ideal operation of the equipment on the platform.

Example Application

Moving from the architectural view of a motion control system in Figure 1, valuable definitions and insights also come from analyzing application-specific, physical attributes. Consider the system in Figure 2, which offers a conceptual view of an automated inspection system for a production line. This camera system inspects items that move in and out of its field of view on a conveyor belt. In this arrangement, the camera attaches to the ceiling through a long bracket, which establishes its height (see D in Figure 2), in order to optimize its field of view for the size of the objects it will inspect. Since factories are full of machinery and other activity, the

camera can experience swinging motion (see $\varphi_{SW}(t)$ in Figure 2) at times, which can cause distortion in the inspection images. The red dotted lines in this diagram provide an exaggerated view of total angular error ($\pm\varphi_{SW}$) that comes from this swinging motion and the green dotted lines represent the level of angular error that will support the system's image quality objectives ($\pm\varphi_{RE}$). The view in Figure 2 defines the key system-level metric (image distortion) in terms of linear displacement error (d_{SW}, d_{RE}) on the inspection surface. These attributes relate to the camera height (D) and the angular error terms (φ_{SW}, φ_{RE}) through a simple trigonometric relationship in Equation 1.

$$\begin{aligned} d_{SW} &= D \times \sin(\varphi_{SW}) \\ \varphi_{SW} &= a\sin\left(d_{SW}/D\right) \\ d_{RE} &= D \times \sin(\varphi_{RE}) \\ \varphi_{RE} &= a\sin\left(d_{RE}/D\right) \end{aligned} \quad (1)$$

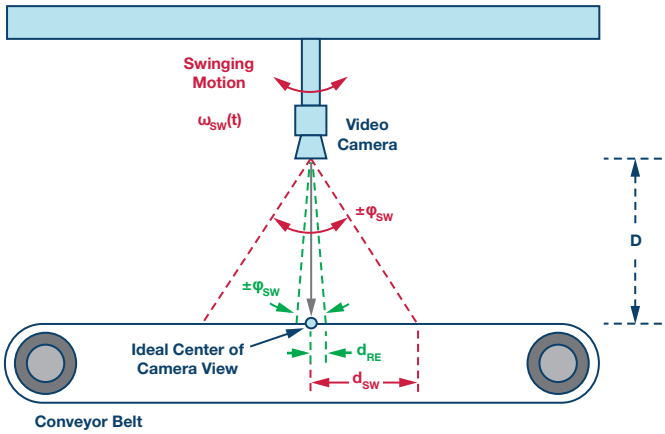

Figure 2. Industrial camera inspection system.

The most applicable motion control technique for this type of system is known as *image stabilization*. Early image stabilization systems used gyroscope-based feedback systems to drive servo motors, which adjust the orientation of the image sensor during the time that the shutter is open. The emergence of MEMS technology helped reduce the size, cost, and power of these functions in a revolutionary manner, which led to wider spread use of this technique in modern day digital cameras. Advances in digital image processing techniques, which still use MEMS-based angular rate measurements in their algorithms, have led to elimination of the servo motor in many applications. Whether the image stabilization comes from a servo motor or through digital post processing of image files, the fundamental function (feedback sensing) of the gyroscope remains the same, as does the consequence of its noise. For simplicity, this discussion focuses on the classic approach (servo motor on the image sensor) to explore the most relevant noise fundamentals, and how they relate to the most important physical attributes of this type of application.

Angle Random Walk (ARW)

All MEMS gyroscopes have noise in their angular rate measurements. This inherent sensor noise represents the random variation in the gyroscope's output, when it is operating in static inertial (no rotational motion) and environmental conditions (no vibration, shock, etc.). The most common metrics that MEMS gyroscope data sheets offer to describe their noise behaviors are *rate noise density* (RND) and *angle random walk* (ARW).

The RND parameter typically uses units of °/sec/$\sqrt{\text{Hz}}$ and provides a simple way to predict the total noise, in terms of angular rate, based on the gyroscope's frequency response. The ARW parameter typically uses units of °/$\sqrt{\text{hour}}$ and is often more useful when analyzing the impact that noise has on angle estimation over specific periods of time. Equation 2 offers a generic formula for estimating the angle, based on the angular rate measurement. In addition, it also provides a simple formula that relates the RND parameter to the ARW parameter. This relationship represents a small adaption (single-sided vs. double-sided FFT) from the one in IEEE-STD-952-1997 (Appendix C).

$$\begin{aligned} \varphi_n(t) &= \int_0^{\tau} \omega_n(t) \times dt \\ \varphi_n(\tau) &= ARW \times \sqrt{\tau} \\ ARW &= \frac{60}{\sqrt{2}} \times RND \\ \varphi_n(\tau) &= \frac{60}{\sqrt{2}} \times RND \times \sqrt{\tau} \end{aligned} \quad (2)$$

Figure 3 provides a graphical reference, which helps support further discussion of the behavior that the ARW parameter represents. The green dotted lines in this illustration represent the ARW behavior when the gyroscope has an RND of 0.004°/sec/$\sqrt{\text{Hz}}$, which equates to an ARW of 0.17°/$\sqrt{\text{hour}}$. The solid lines represent six separate integrations of this gyroscope's output, over a period of 25 ms. The random nature of the angular errors, with respect to time, show that the ARW's primary utility is in estimating the statistical distribution of the angular errors over a specific integration time. Also note that this type of response does assume the use of high-pass filtering to remove initial bias errors in the integration process.

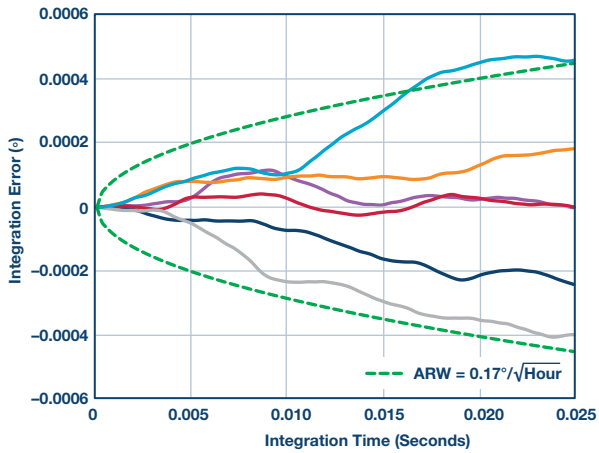

Figure 3. Angle random walk (ADIS16460).

Relating back to the application example in Figure 2, combining Equations 1 and 2 provides an opportunity to relate important criteria (physical distortion on the inspection surface) to noise performance metrics (RND, ARW) that are commonly available in MEMS gyroscope data sheets. In this process, assuming that the integration time (τ) from Equation 1 is equal to the image capture time provides another simplification that might be useful. Equation 3 applies the generic relationship from Equation 1 to estimate that when the camera is 1 meter (D) off of the inspection surface and the maximum allowable distortion error is 10 µm (d_{RE}), the angular error from the gyroscope (φ_{RE}) must be less than 0.00057°.

$$\begin{aligned} d_{RE} &= D \times \sin(\varphi_{RE}) \\ \varphi_{RE} &\le \arcsin\left(d_{RE}/D\right) \\ \varphi_{RE} &\le \arcsin\left(0.00001m/1m\right) \\ \varphi_{RE} &\le 0.00057° \end{aligned} \quad (3)$$

Equation 4 combines the results from Equation 3 and the generic relationship in Equation 2 to predict ARW and RND requirements for the MEMS gyroscope in a particular situation. This process assumes that the image capture times of 35 ms represents the integration time (τ) from Equation 2, which leads to predicting that the gyroscope's ARW needs to be less than $0.18°/\sqrt{hour}$, or the RND must be less than $0.0043°/sec/\sqrt{Hz}$ to support this requirement. Of course, this may not be the only requirement that these parameters support, but these simple relationships do provide an example of how to relate to known requirements and conditions.

$$\varphi_{RE} \le \varphi_n \le 0.00057°$$

$$\varphi_n \le 0.0057°$$

$$ARW \times \sqrt{\tau} \le 0.00057°$$

$$ARW \times \le \frac{\sqrt{2} \times 0.00057°}{\sqrt{\tau}}$$

$$RND \le \frac{\sqrt{2} \times 0.00057°}{60 \times \sqrt{\tau}}$$

When τ can reach 0.035 seconds

$$ARW \times \le \frac{0.00057°}{\sqrt{\frac{0.035 \text{ seconds}}{3600 \text{ seconds}/hour}}} \quad (4)$$

$$ARW \times \le 0.18 \, {}^{\circ}/\sqrt{hour}$$

$$RND \le 0.18 \, {}^{\circ}/\sqrt{hour} \times \sqrt{2}/60$$

$$RND \le 0.0043 \, {}^{\circ\text{sec}}/\sqrt{Hz}$$

Angular Rate Noise vs. Bandwidth

Those who are developing systems that provide continuous pointing control may prefer to evaluate the noise impact in terms of angular rate, since they may not have a fixed integration time to leverage the ARW-based relationship. Evaluating the noise in terms of angular rate often involves some consideration of the RND parameter and the frequency response in the gyroscope's signal chain. The gyroscope's frequency response is often most influenced by filtering, which supports application-specific requirements for loop stability criteria and rejection of undesirable sensor response to environmental threats, such as vibration. Equation 5 provides a simple way to estimate the noise associated with a particular frequency response (noise bandwidth) and RND.

$$TN = \text{Total Noise}, \, {}^{\circ}/\text{sec} \; (rms)$$

$$TN = RND \times \sqrt{f_{NBW}}$$

$$where: \quad (5)$$

$$RND = \text{Rate Noise Density}, \, {}^{\circ\text{sec}}/\sqrt{Hz}$$

$$f_{NBW} = \text{Noise Bandwidth, Hz}$$

When the RND's frequency response follows a single-pole or double-pole, low-pass filter profile, the noise bandwidth (f_{NBW}) relates to the filter cutoff frequency (f_C) according to the relationships in Equation 6.

$$f_{NBW} = 1.57 \times f_C \text{ (single-pole, low-pass filter)}$$
$$f_{NBW} = 1.22 \times f_C \text{ (double-pole, low-pass filter)} \quad (6)$$

For example, Figure 4 offers two different spectral plots for the noise in the ADXRS290, which has an RND of $0.004°/sec/\sqrt{Hz}$. In this plot, the black curve represents the noise response when using a double-pole, low-pass filter, which has a cutoff frequency of 200 Hz filter, while the blue curve represents the noise response when using a single-pole, low-pass filter, which has a cutoff frequency of 20 Hz filter. Equation 7 provides calculations for the total noise of each of these filters. As expected, the 200 Hz version has higher noise than the 20 Hz version.

$$TN = RND \times \sqrt{1.22 \times f_C}$$

$$TN_{200\,Hz} = 0.004 \, {}^{\circ\text{sec}}/\sqrt{Hz} \times \sqrt{1.22 \times 200}$$

$$TN_{200\,Hz} = 0.062 \, {}^{\circ}/\text{sec} \quad (7)$$

$$TN_{20\,Hz} = 0.004 \, {}^{\circ\text{sec}}/\sqrt{Hz} \times \sqrt{1.57 \times 20}$$

$$TN_{20\,Hz} = 0.022 \, {}^{\circ}/\text{sec}$$

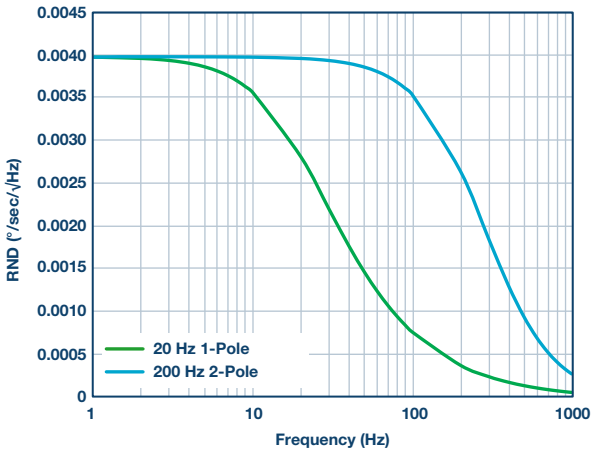

Figure 4. ADXRS290 noise density with filters.

In cases where the system requires custom filtering, whose frequency response ($H_{DF}(f)$) does not fit the simple single-pole and double-pole models in Equations 6 and 7, Equation 8 offers a more generic relationship for predicting the total noise:

$$TN = \sqrt{\int_0^F [RND^2(f) \times H_{DF}{}^2(f)] \times df} \quad (8)$$

In addition to influencing the total angular rate noise, gyroscope filters also contribute phase delay to the overall loop response, which has a direct impact on another important figure of merit in feedback control systems: phase margin at the unity-gain crossover frequency. Equation 9 offers a formula for estimating the phase delay (θ) that a single-pole filter (f_C = cutoff frequency) will have on the control's loops frequency response, at its unity-gain crossover frequency (f_G). The two examples in Equation 9 illustrate the phase delay at a unity-gain crossover frequency of 20 Hz, for filters with cutoff frequencies of 200 Hz and 60 Hz, respectively. This impact on phase margin can lead to specifying gyroscope bandwidths that are 10× greater than the unity-gain crossover frequency, which can place even more emphasis on selecting a MEMS gyroscope with favorable RND levels.

$$\theta(f_G, f_C) = \text{a tan}\left(\frac{f_G}{f_C}\right)$$

$$\theta(20, 200) = \text{a tan}\left(\frac{20}{200}\right) = \sim 5.7° \quad (9)$$

$$\theta(20, 60) = \text{a tan}\left(\frac{20}{60}\right) = \sim 18.4°$$

Modern control systems often leverage digital filters, which may have different models for predicting their phase delay at critical frequencies for the control loop. For example, Equation 10 presents a formula for predicting the phase delay (θ) associated with a 16-tap FIR filter (N_{TAP}), which is running at the 4250 SPS (f_S) update rate of the ADXRS290, at the same unity-gain crossover frequency (fG) of 20 Hz. This type of relationship can help in determining the total number of taps that a system architecture can allow for this type of filter structure.

$$\theta = \frac{N_{TAP} + 1}{2} \times \left(\frac{f_G}{f_C}\right)$$
$$\theta = \frac{16 - 1}{2} \times \left(\frac{20}{4250}\right) \times 360° \quad (10)$$
$$\theta = 12.7°$$

Conclusion

The bottom line is that noise in the angular rate feedback loops can have a direct influence on key performance criteria in motion control systems, so it should be a consideration as early as possible in the design process for a new system. Those who can quantify how angular rate noise will influence system-level behaviors will have a significant advantage over those who only know that they need low noise. They will be able to establish performance goals that create observable value in their applications, and they will be in an excellent position to quantify system-level consequences when other project objectives encourage consideration of a specific MEMS gyroscope. Once that basic understanding is in place, system designers can focus on identifying a MEMS gyroscope that meets their performance requirements, using bandwidth, rate noise density, or angle random walk metrics to guide their consideration. As they look to optimize the noise performance that they realize from the sensors they select, they can use the relationships with bandwidth (angular rate noise) and integration time (angle error) to drive other important system-level definitions that will support the most appropriate performance for the application.

About the Author

Mark Looney [*mark.looney@analog.com*] is an *i*Sensor® applications engineer at Analog Devices in Greensboro, North Carolina. Since joining ADI in 1998, he has accumulated experience in sensor-signal processing, high speed analog-to-digital converters, and dc-to-dc power conversion. He earned B.S. (1994) and M.S. (1995) degrees in electrical engineering from the University of Nevada, Reno, and has published several articles. Prior to joining ADI, he helped start IMATS, a vehicle electronics and traffic solutions company, and worked as a design engineer for Interpoint Corporation.

Online Support Community

Engage with the Analog Devices technology experts in our online support community. Ask your tough design questions, browse FAQs, or join a conversation.

ez.analog.com

Analog Devices, Inc.
Worldwide Headquarters

Analog Devices, Inc.
One Technology Way
P.O. Box 9106
Norwood, MA 02062-9106
U.S.A.
Tel: 781.329.4700
(800.262.5643, U.S.A. only)
Fax: 781.461.3113

Analog Devices, Inc.
Europe Headquarters

Analog Devices, Inc.
Wilhelm-Wagenfeld-Str. 6
80807 Munich
Germany
Tel: 49.89.76903.0
Fax: 49.89.76903.157

Analog Devices, Inc.
Japan Headquarters

Analog Devices, KK
New Pier Takeshiba
South Tower Building
1-16-1 Kaigan, Minato-ku,
Tokyo, 105-6891
Japan
Tel: 813.5402.8200
Fax: 813.5402.1064

Analog Devices, Inc.
Asia Pacific Headquarters

Analog Devices
5F, Sandhill Plaza
2290 Zuchongzhi Road
Zhangjiang Hi-Tech Park
Pudong New District
Shanghai, China 201203
Tel: 86.21.2320.8000
Fax: 86.21.2320.8222

analog.com

ANALOG DEVICES
AHEAD OF WHAT'S POSSIBLE™